Simulations Reveal Different Particle Trapping Mechanisms in Spatially Ordered and Disordered Interacting Gels

Johann Hansing, Roland R. Netz

Freie Universität Berlin

March 16, 2018

Author Information

Johann Hansing
Fachbereich Physik
Freie Universität Berlin
Arnimallee 14
14195 Berlin
Phone: +49 (0)30/838-57634
E-mail: johannh@zedat.fu-berlin.de

Corresponding Authors

johannh@zedat.fu-berlin.de

Abstract

Using stochastic simulations we study the influence of spatial disorder on the diffusion of a single particle through a gel that consists of rigid straight fibers. The interaction between the particle and the gel fibers consists of an invariant short-range repulsion, the steric part, and an interaction part that can be attractive or repulsive and of varying range. The effect spatial disorder has on the particle diffusivity depends crucially on the presence of non-steric interactions. For attractive interactions, disorder slows down diffusion. The reason is that in disordered gels the particle becomes strongly trapped in regions of locally increased fiber density. For repulsive interactions, the diffusivity is minimal for intermediate disorder strength, since highly disordered lattices exhibit abundant passageways of locally low fiber density. The comparison with experimental data on protein and fluorophore diffusion through various hydrogels is favorable. Our findings shed light on particle diffusion mechanisms in biogels an thus on biological barrier properties which can be helpful for the optimal design of synthetic diffusors as well as synthetic mucus constructs.

1 Introduction

Hydrogels like mucus, the extracellular matrix (ECM) and the nuclear pore complex form natural barriers for pathogens and play an important role in regulating the exchange of molecules and particles between organelles and cells [1]. Even though the filtering capabilities of such hydrogels are of high importance for biological function, they are still not fully understood. Numerous experimental and theoretical studies investigated the mechanisms that determine the mobility of particles inside gels, as one main result it was found that nonsteric interactions between the gel and the diffusing particle, which can be attractive or repulsive, are a major factor in addition to purely steric obstruction effects. Electrostatic interactions in particular determine the mobility of charged particles in mucus [1–10], the ECM [1, 11–13] and bacterial biofilms [14]. Charge is also suggested to be a main ingredient regulating diffusion through the nuclear pore complex [1, 15]. Regarding the sign of the electrostatic interactions, a number of experimental papers report different diffusive behavior for positively and negatively charged particles in gels that have a given net charge [5–7, 16, 17]. We previously have investigated diffusion of spherical particles in an ordered cubic lattice of rigid cylindrical fibers as a model for the polymer network [16, 18]. Straight rigid fibers have been used successfully to model the stiff collagen network of the ECM [19, 20] and mucus [18]. For mucus, recent experimental research has shown that the movement of nanoparticles is obstructed by a relatively rigid polymer scaffold [21]. Furthermore, single particle tracking reveals that some particles are almost completely immobilized in mucus inside a small volume, while other of the same type are mobile [4,11] indicating that the confined by the rigid mucus fibers, whereas the former are mobile inside larger pockets of the polymer lattice. In our previous model we included the effect of attractive versus repulsive interactions on particle diffusivity with an exponentially screened interaction potential between the fibers and the particle [16, 18]. With our simple model gel, we showed that nonsteric interactions determine the effective particle diffusivity in a crucial fashion and usually dominate over steric hindrance effects. In particular, we showed the particle filtering to be charge asymmetric, meaning that particles are more strongly immobilized in oppositely charged gels, i.e. for attractive interactions, than in similarly charged gels, in agreement with experimental findings [5–7,16,17]. Other pertinent theoretical studies on particle diffusion in crowded media are [19, 20, 22–27]. In this paper, we generalize our model and consider disordered fiber lattices and in particular the transition from ordered cubic to spatially disordered gels in combination with attractive and repulsive nonsteric as well as steric interactions.

Our main results are as follows: While particle diffusion in purely steric gels depends only weakly on the spatial arrangement of the fibers if the particle is smaller than the mesh size, in accordance to previous theoretical results [19, 26, 27], the diffusive behavior in the presence of long-ranged, nonsteric interactions between particle and fibers depends drastically on the presence of spatial disorder of the gel. In particular, for attractive nonsteric particle-gel interactions we find different particle trapping mechanisms for spatially ordered and disordered gels. In highly ordered gels, particles are attracted to the vertices of the cubic fiber lattice where they become immobilized for small fiber volume fractions. In contrast, in disordered gels, regions of high local fiber density form trapping areas that strongly attract and thereby immobilize the particle very effectively, as has previously been proposed on the basis of experimental findings [3,12]. The influence of gel disorder is less pronounced for repulsive nonsteric interactions. To test our model, we compare our simulated particle diffusivities with previously published experimentally measured diffusivities of different particles in different biogels. For negatively charged Alexa488 fluorophore molecules in gels consisting of neutral, positive and negative dextran polymers [16] we find good qualitative agreement between experiment and simulation as a function of the fiber volume fraction.

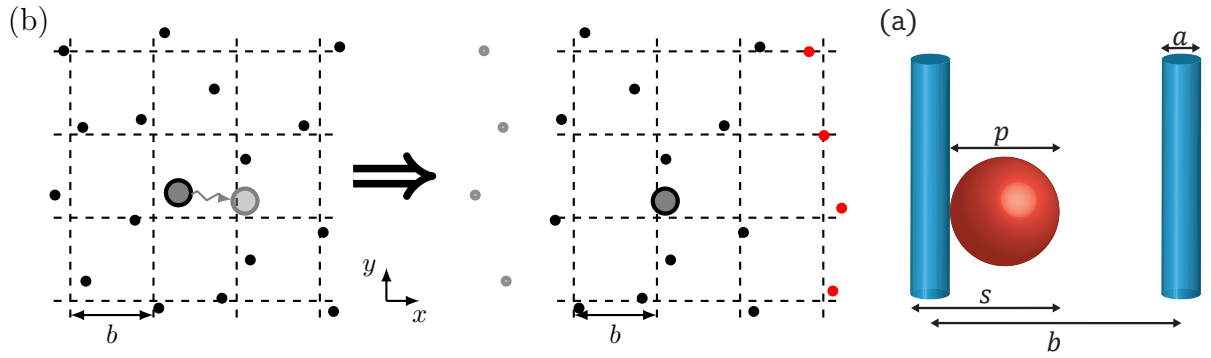

Figure 1. (a) The black dots indicate the positions of the fibers parallel to the z-axis. In the presence of spatial disorder, the fibers are displaced from their positions on the reference square lattice of spacing b by Gaussian random numbers with a standard deviation of $\sigma_d/b = 0.2$. The diffusing particle, drawn as a circle, crosses the boundary of the central cell in x-direction (left figure). In the simulation model, when this happens, the gray fibers to the left are removed and the red fibers are added at the right boundary (right figure). (b) Schematic definition of the particle diameter p, the fiber diameter a, the steric diameter $s = a + p$ and the gel mesh size b.

2 Model

The diffusive motion of the particle is governed by the overdamped Langevin equation

$$\dot{r}_i(t) = -\mu_0\, \partial_i U(\vec{r}(t)) + \zeta_i(t)\,, \quad (i = x, y, z)\,, \tag{1}$$

where $\dot{r}_i$ is the particle velocity, ∂_i the spatial derivative, U is the potential and μ_0 the bulk particle mobility. The random velocity ζ_i is a stochastic variable, modeled with Gaussian white noise

$$\langle \zeta_i(t) \rangle = 0\,, \tag{2}$$

$$\langle \zeta_i(t)\, \zeta_j(t') \rangle = 2\mu_0 k_B T\, \delta(t - t')\, \delta_{ij}\,, \tag{3}$$

where δ_{ij} is the Kronecker delta, $k_B T$ is the thermal energy and the indices i, j denote Cartesian components. Since we are interested in the long-time diffusivity of the particle, the particle mass is neglected in the equation of motion (1). By discretizing the Langevin equation with time step Δt, an iterable equation for the change of the particle position is obtained,

$$\Delta\tilde{r}_i = -\tilde{\mu}\, \tilde{\partial}_i \tilde{U} + \sqrt{2\tilde{\mu}}\, \tilde{\zeta}_i\,, \tag{4}$$

where $\Delta\tilde{r}_i$ is the displacement of the particle and $\tilde{\zeta}$ is a Gaussian distributed random number with zero mean and variance $\langle \tilde{\zeta}_i\, \tilde{\zeta}_j \rangle = \delta_{ij}$. The tilde indicates rescaled variables. The potential $\tilde{U}$ is rescaled by the thermal energy $k_B T$ and all lengths $\tilde{r} = r/b$ are rescaled by the mesh size b (c.f. fig. 1a). The rescaled timestep is defined as

$$\tilde{\mu} = \frac{\Delta t\, \mu_0\, k_B T}{b^2}\,. \tag{5}$$

For the simulations a small enough rescaled time step $\tilde{\mu}$ must be chosen. We tested different time steps and found no increase in accuracy for $\tilde{\mu} < 5 \times 10^{-6}$. To ensure that we are within the continuum limit we chose $\tilde{\mu} = 10^{-6}$ for all data presented in this work.

The diffusivity D of the particle is obtained by linearly fitting the mean-squared displacement in the long-time limit according to

$$\lim_{t\to\infty} \langle \Delta r^2(t) \rangle \;=\; 6D\,t\;, \tag{6}$$

where $\Delta r^2(t) = (\vec{r}(t) - \vec{r}(0))^2$. The diffusivity of the particle if no gel is present is denoted by $D_0 = \mu_0\, k_B T$. For each data point, we perform one simulation of a single long particle trajectory of at least 10^9 steps. Due to the stochastic nature of our simulations, the relative diffusivities fluctuate. Sample repeat simulations have shown that the error for D/D_0 is about 5%+0.001. In the supplementary information in fig. S1, we show that the long-time limit in eq. (6) is always reached in our simulations.

The simulated gel consists of 48 fibers, i.e. 16 fibers parallel to each axis x, y and z. We introduce spatial disorder by displacing the fibers from positions on a reference cubic lattice. The displacement of each fiber is a random vector orthogonal to the fiber axis, sampled from a Gaussian distribution with zero mean and standard deviation σ_d. In fig. 1a we present a sketch of our model for $\sigma_d/b = 0.2$, the reference cubic lattice with mesh size b is indicated by dashed lines. When the particle leaves the central cell of the reference cubic lattice, the eight distal fibers are removed and eight new fibers are added on the other side. This process is illustrated in fig. 1a for a particle in the xy-plane that leaves the central cell in the positive x-direction. Thus, in our simulation model, the gel changes as the particle moves across cells.

Steric hindrance between the particle and the fibers is modeled by a truncated, shifted Lennard Jones potential

$$U_{\text{steric}}(\vec{r}) = \sum_{n=1}^{48} \begin{cases} 4\epsilon \left[\left(\frac{s}{2\rho_n}\right)^{12} - \left(\frac{s}{2\rho_n}\right)^{6} + \frac{1}{4} \right], & \rho_n \le 2^{-5/6} s \\ 0\,, & \rho_n > 2^{-5/6} s\,, \end{cases} \tag{7}$$

where the energy parameter is fixed at $\epsilon = 1\ k_B T$, ρ_n is the distance between the particle and the nth fiber and $s = a + p$ is the steric diameter, i.e. the sum of the diameters of the fibers a and the particle p, as shown in fig. 1b. The long-ranged nonsteric interaction potential between the fibers and the particle is defined as

$$U_{\text{int}}(\vec{r}) = \sum_{n=1}^{48} U_0 \exp\left(-\frac{\rho_n}{k}\right)\;, \tag{8}$$

where k is the interaction range and U_0 the strength of the potential. For negative U_0 the potential is attractive and for positive U_0 it is repulsive. For electrostatic interactions k corresponds to the Debye screening length [28]

$$k^{-2} = 4\pi l_B I\,, \tag{9}$$

where $l_B = e^2/4\pi\varepsilon k_B T$ is the Bjerrum length, e is the elementary charge and ε the permittivity. $I = \frac{1}{2}\sum_j n_j\, z_j^2$ is the ionic strength and z_j the valence of salt ion j and n_j its number density. The salt number density n is related to the molar ion concentration C_{Ion} through $C_{\text{Ion}} = n/N_A$, where N_A is the Avogadro constant. U_0 can be interpreted as the product of the particle charge and the linear polymer charge density [18]. Thus, eq. (8) becomes an effective electrostatic interaction potential between charged fibers and charged particle. Following our previous research on particle diffusion in interacting gels [16, 18] we neglect hydrodynamic interactions.

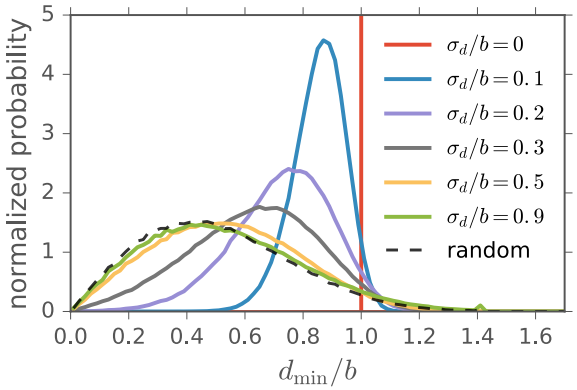

Figure 2. Distribution of the smallest distance $d_{\min}$ between parallel fibers for different disorder strengths σ_d. For $\sigma_d/b = 0$ the smallest distance is b and the distribution is a delta peak. The dashed line is the distribution for 16 parallel fibers that are placed on a $3b \times 3b$ square at random positions, which agrees with the distribution for $\sigma_d/b = 0.9$.

3 Results

Before we discuss the resulting particle diffusivity D, we characterize the spatial gel structure for different disorder strengths σ_d. To illustrate the transition from a completely ordered gel, $\sigma_d/b = 0$, to a highly disordered gel, $\sigma_d/b = 0.9$, we show the distribution of the smallest distances $d_{\min}$ between parallel fibers for different σ_d in fig. 2. For the ordered gel, $\sigma_d = 0$, the distribution corresponds to a δ-peak. For increasing σ_d, $d_{\min}$ becomes more broadly distributed. The dashed line in fig. 2 corresponds to the distribution for 16 parallel fibers that are placed within a $3b \times 3b$ square at uniformly distributed random positions, which agrees with the distribution for $\sigma_d/b = 0.9$ (green line). Thus, the value $\sigma_d/b = 0.9$ corresponds practically to an uncorrelated fiber placement. In fig. S2 in the supplementary information, we also investigate the effect of changing the central cell size, which determines at which particle positions the fiber network is partially rebuilt (c.f. fig. 1a), for systems with strong interaction disorder $\sigma_d/b \geq 0.5$.

The presentation of our simulation results is organized as follows. First, we examine diffusion in purely steric gels and compare our modeling results to experimental data. After this we investigate how disorder affects the diffusivity in the presence of long-ranged interactions between the particle and the gel and again compare with experimental data.

3.1 Purely steric gels

In fig. 3a we present the relative particle diffusivity D/D_0 as a function of the fiber volume fraction ϕ for purely steric gels where $U_0 = 0$ for various disorder strengths σ_d. The second x-axis at the top indicates the rescaled steric diameter $s/b = (a+p)/b$. The fiber volume fraction is given by

$$\phi = 3\pi(a/2b)^2 \tag{10}$$

and depends on the fiber diameter a, in order to present our results as a function of the volume fraction we thus have to make a specific choice for the value of a. In fig. 3a we use a small fiber particle size ratio $a/p = 0.05$, so in the numerical simulations, the fibers are very thin lines. Experimentally, a ratio of $a/p = 0.05$ corresponds to a particle diameter p of $60 - 200$ nm for a fiber diameter a of $3 - 10$ nm for mucin [29]. This means that for mucus the mesh size b in fig. 3a is between ~ 50 nm for large ϕ and

$\sim$ 1000 nm for small ϕ. Note, that to simulate a different combination of biogel and particle, one only has to adapt the ratio a/p, which determines the ϕ via eq. (10). For the completely ordered cubic lattice with $\sigma_d/b = 0$, the diffusivity becomes zero for $s > b$ ($\phi > 0.0053$), since the particle can not move between adjacent fibers anymore [18]. For increasing disorder $\sigma_d > 0$ this complete immobilization of the particle for $s > b$ is prevented. If the particle encounters an impasse, it will eventually return and the fiber lattice in the cell is partially rebuilt (c.f. fig. 1a). As a consequence, the particle has a finite mobility even at large ϕ for $\sigma_d > 0$. In fig. 3b we plot the diffusivities as a function of the effective volume fraction ϕ_{eff}, which is the ratio of the gel volume that is accessible to the center of the particle to the total volume. We determine ϕ_{eff} by Monte-Carlo integration, similar to [26]. For 200 consecutive times during a single simulation, 10^6 random points are sampled to check whether they collide with one of the fibers. For the $\sigma_d/b = 0$ data the effective volume fraction is given analytically by $\phi_{\text{eff}} = (3\pi b a^2/4 - \sqrt{2}a^3)/b^3$. Figure 3b demonstrates that the data collapses onto a master curve, i.e., that the effects of the spatial disorder almost disappear in this representation, similar to previous findings [26]. Thus, a diffusion model based on the free volume describes particle diffusion in disordered purely steric gels very nicely.

Figure 3a includes the previously suggested scaling function [30]

$$D/D_0 = \exp(-0.84[\phi(1 + p/a)^2]^{1.09}) \,, \tag{11}$$

which is a heuristic fit to Brownian dynamics simulations for spherical particles in gels of randomly oriented, rigid straight fibers and has been shown to agree with various other simulation data as well [31]. We find that our simulation results agree perfectly with eq. (11) for an intermediate value $\sigma_d/b = 0.5$. This indicates that our disordered gel model has similar diffusion properties as a model with random fiber orientations, in accordance to the findings by Masoud and Alexeev who have demonstrated that for purely steric random gels the diffusivity is almost independent of the exact fiber lattice geometry [27].

In fig. 3c we compare our diffusivity results to a general stretched exponential dependency

$$D/D_0 = \exp(-\alpha\phi^n) \,, \tag{12}$$

where we show the logarithm of D/D_0 in a log-log plot. As indicated by the straight lines, the exponent n varies from $n = 1.04 \pm 0.04$ for $\sigma_d/b = 0.9$ to $n = 1.14 \pm 0.06$ for $\sigma_d/b = 0.5$ (c.f. table 1) for highly disordered gels, and thus is very close to the exponent $n = 1.09$ in eq. (11). In contrast, for most experimental data, the stretched-exponential parameter is between $n = 0.5$ and 1 [16,32–34]. We are aware of only one experimental study that reports larger n values in the range of 1.1 to 2.4 for different probes in PDMS solution [35].

Note to Roland - All three referees commented on this part: ref 1: it is not clear how the hydrodynamic interactions could potentially result in the decrease of the scaling exponent, I think it should be another way around. ref 2: [...] (ref. 26,30) is the gel model network the same in these references? Would this influence the result? ref 3: [...] could an analysis be done to determine quantitatively when hydrodynamics play a role and how much influence they have on the particle diffusivity.

Phillips and colleagues have published numerous papers on the effect of HI on purely steric gels [31,36–38]. They found that the effect of HI can approximately be taken into account by multiplying the diffusivity for simulations without HI D_{noHI}/D_0 (the steric part) with the spatially averaged short-time relative diffusion coefficient $\langle D_s \rangle / D_s^0 \rangle$ of the system (the hydrodynamic part), i.e. $D/D_0 = D_{\text{noHI}}/D_0 \times \langle D_s \rangle / D_s^0 \rangle$. For gels of disordered, randomly oriented straight fibers they propose the following expression [31]:

$$D/D_0 = \exp(-\lambda\phi^m) \, \exp(-[0.84(1 + p/a)^2 \, \phi]^{1.09}) \,, \tag{13}$$

Table 1. The parameters of a stretched exponential fit, eq. (12), to the data presented in figs. 3a and 3c. The errors corresponds the estimated standard deviations of the fit parameters.

σ_d/b	0	0.1	0.2	0.3	0.5	0.9
$\alpha \times 10^{-3}$	4 ± 3	2 ± 1	1.9 ± 0.7	1.0 ± 0.4	0.8 ± 0.2	0.35 ± 0.08
n	1.4 ± 0.2	1.3 ± 0.2	1.3 ± 0.1	1.16 ± 0.07	1.14 ± 0.06	1.04 ± 0.04

where the the first exponential is the hydrodynamic part and the second exponential is the steric part. Note that the steric part corresponds to Johnson's function in eq. (11). λ and m are listed for different ratios $0.1 < a/p < 2$ in [31]. Figure 3a shows a line for eq. (13). Comparing the lines for Johnson's (eq. (11)) and Phillips function, one can see that the diffusivities are significantly smaller without HI, but the qualitative behavior remains the same. According to eq. (13), the effect of HI increases monotonically with increasing fiber volume fraction ϕ for purely steric gels. In fig. 3c a we include a line for eq. (13). The line has a scaling exponent of about $n \sim 0.35$ (upper black line), which corresponds to the scaling exponent m from eq. (13) for small ratios $a/p = 0.05$. In other theoretical a scaling exponent of $n \sim 0.7$ was reported for simulations with HI and random, cross-linked fiber networks with different cross-linking densities and $a/p = 0.5$ and 0.3 [27]. Thus, we conclude that the increased value of n in our simulations in comparison to most experiments can likely be attributed to the lack of hydrodynamic effects in our model. However, it is unclear if for our simulations n will be the same as for eq. (13), $n \sim 0.35$, since we employ a different fiber network with parallel an orthogonal fibers. Furthermore, the method of adding the effect of HI to the diffusivity for purely steric system has, to our knowledge, not yet been verified by comparing eq. (13) to simulations with HI.
Comparisons to experimental data are presented in fig. 4. Figure 4a shows results for RNAse diffusion in polyacrylamide gel with a diameter ratio $a/p = 0.32$ by Tong and Anderson [39], fig. 4b for BSA diffusion in polyacrylamide gel with a ratio $a/p = 0.18$ by Tong and Anderson and Park et al. [39,40] and fig. 4c for BSA diffusion in calcium alginate with a ratio $a/p = 0.1$ by Amsden [41]. The estimated a/p fiber-particle diameter ratios are taken from [31]. We find qualitative agreement between simulation and experiment in all three cases for highly disordered gels with $\sigma_d/b = 0.9$ and 0.5. For large ϕ the experimental and the simulation data agree quantitatively in figs. 4 b and c, this indicates that hydrodynamic interactions are irrelevant compared to steric hindrance effects for these dense systems. In contrast, at low ϕ our simulation model overestimates the diffusivity, presumably due to the lack of hydrodynamic interactions [31]. We conclude that the difference of the stretched-exponential parameters n extracted from our simulations ($n \sim 1.1$) versus experiments ($n \sim 0.7$) is mainly reflected by the deviation between experimental and simulated diffusivities at small to intermediate volume fractions. For ordered gels with $\sigma_d/b = 0$, we find strong disagreement between simulation and experiment, in particular at large volume fractions ϕ. This indicates that the gels used in the experiment are quite disordered and that our disorder model correctly describes the experimental gel structures.

3.2 Interacting gels

We move on to interacting gels. In figs. 5 and 6 we present the diffusivity D/D_0 as a function of the fiber volume fraction ϕ for repulsive and attractive interaction potential strength $U_0 = 10 k_B T$ and $U_0 = -10 k_B T$. The rescaled interaction range is $k/s = 0.5$ in fig. 5 and $k/s = 1.5$ in fig. 6. With the exception of fig. 5a we find the following behavior: In ordered gels, the particle diffusivity D exhibits a non-monotonic dependence on ϕ, whereas in disordered gels D decreases monotonically and steeply already at small ϕ. The non-monotonicity of D for ordered gels can be explained as follows. For increasing ϕ and fixed interaction

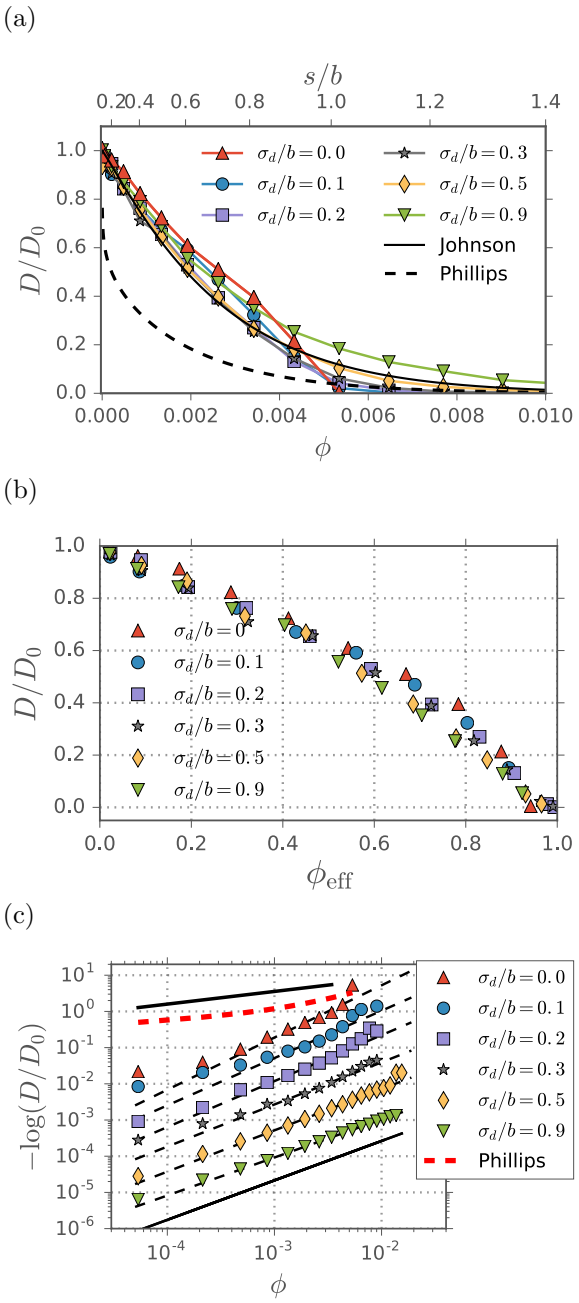

Figure 3. (a) Particle diffusivity in a purely steric gel as a function of the fiber volume fraction ϕ for a diameter ratio $a/p = 0.05$ and different disorder strengths σ_d. The plot includes an upper x-axis for the steric diameter s/b defined in fig. 1b. The continuous black line denotes the scaling function eq. (11), the dashed black line eq. (13). We find particularly good agreement with our data for disorder strength $\sigma_d/b = 0.5$. (b) Particle diffusivity as a function of the effective fiber volume fraction ϕ_{eff} defined in the text for different σ_d, exhibiting collapse onto a master curve. In (c), the same data as in (a) is presented in a log-log versus log plot, shifted along the y-axis to avoid overlapping curves. The dashed straight lines are stretched exponential fits according to eq. (12), the fit parameters are given in table 1. The solid straight line indicates $n = 1.09$, the stretched-exponential parameter in eq. (11). The strongly disordered systems with $\sigma_d/b = 0.9$ and $\sigma_d/b = 0.5$ clearly exhibit a stretched exponential scaling. In contrast, for the ordered system with $\sigma_d = 0$ a stretched exponential scaling is only present for intermediate ϕ.

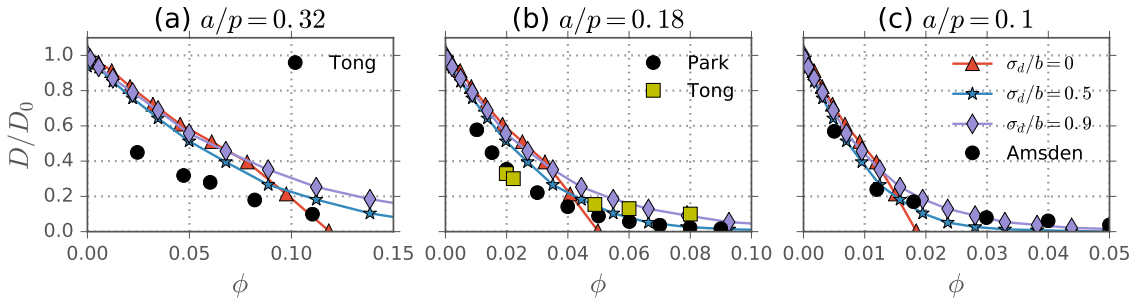

Figure 4. Particle diffusivity in purely steric gels as a function of the fiber volume fraction ϕ from simulations (connected symbols) for ordered ($\sigma_d/b = 0$) and disordered ($\sigma_d/b = 0.5$ and 0.9) gels in comparison to experimental data (unconnected symbols) for: (a) RNAse diffusion in polyacrylamide gel reported by Tong and Anderson [39] with a fiber/particle diameter ratio $a/p = 0.32$ [31]. (b) BSA diffusion in polyacrylamide gel reported by Tong and Anderson [39] and Park et al. [40] with $a/p = 0.18$ [31] and (c) BSA diffusion in calcium alginate gel reported by Amsden [41] with $a/p = 0.1$ [31]. The simulation data is the same in all three subfigures. We find qualitative agreement between our simulation model and the experiments for high disorder parameters $\sigma_d/b = 0.5$ and $\sigma_d/b = 0.9$ and not too low volume fraction.

range k/s, the interaction range relative to the mesh size increases. When the interaction range becomes comparable to the mesh size, roughly at $k/b \approx 0.2$, the interaction potentials of neighboring fibers start to overlap, which creates a rather smooth potential landscape and which thereby leads to an increase in diffusivity with increasing ϕ [18], as can be observed for small ϕ in figs. 5b, 6a and 6b for highly ordered gels. For larger values of ϕ, steric effects become important and give rise to a decrease of D with increasing ϕ. For all results in figs. 5 and 6, increasing the disorder generally leads to a decrease of D with some exceptions that will be discussed below.

Repulsive interactions induce mild exclusion trapping

In gels with repulsive nonsteric interactions the particle experiences mild *exclusion trapping*, i.e. it is confined to the space between the fibers. In ordered gels, $\sigma_d/b < 0.3$, the particle can travel in a relatively unobstructed fashion in between adjacent cells through the centers of the cubic cell faces [18], which is reflected in the high diffusivities in figs. 5a and 6a for particles with a diameter smaller than b which corresponds to $\phi < 0.0053$. For large $\sigma_d/b = 0.9$, the strong disorder creates random passageways of low fiber density, thus in figs. 5a and 6a the particle remains quite mobile even for large $\phi > 0.0053$, when the particle diameter exceeds the mesh size b. Intermediate disorder strengths $0.3 \leq \sigma_d/b \leq 0.5$ lead to the smallest particle mobilities. This non-monotonic dependence on σ_d is also visible in purely steric gels in fig. 3a, but in figs. 5a and 6a it is much more pronounced, due to the additional repulsive interaction potential. The qualitative similarity between purely steric gels and gels with nonsteric repulsive interactions is also apparent when the diffusivity is plotted as a function of the disorder strength in fig. 7.

The different exclusion trapping mechanisms for repulsive interactions can be appreciated from the particle snapshots in fig. 8 for a highly ordered $\sigma_d/b = 0.1$ gel (top left) and a disordered $\sigma_d/b = 0.9$ gel (bottom left). The snap shots correspond to the case of $s = b$ ($\phi = 0.0053$) where the steric diameter is equal to the mesh size so the particle becomes strongly immobilized due to steric hindrance as well as the repulsive interaction effects. Both figures show particle position snap shots clustered in spaces of low local fiber density; for the disordered system, there are fewer and more pronounced clusters in regions that are devoid of fibers. Within these regions, the particle is quite mobile, thus D/D_0 is still relatively high for $\sigma_d/b = 0.9$ and $s = b$ ($\phi = 0.0053$) as seen in figs. 5a and 6a.

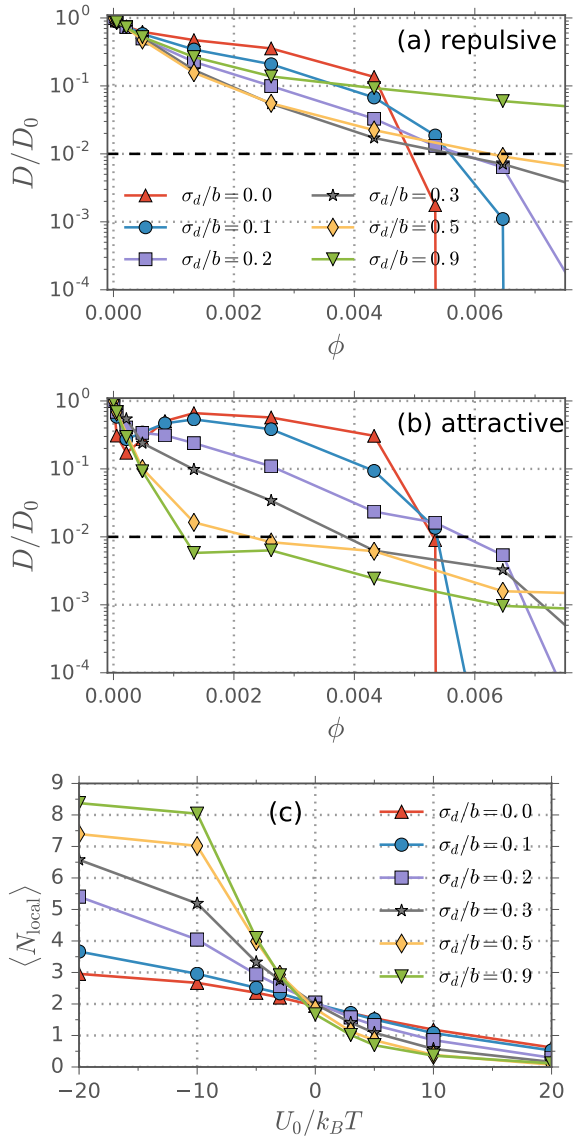

Figure 5. Particle diffusivity in interacting gels as a function of the fiber volume fraction ϕ for a fiber/particle diameter ratio $a/p = 0.05$ and short interaction range $k/s = 0.5$ for different σ_d for (a) repulsive interactions with $U_0 = 10\,k_BT$ and (b) attractive interactions with $U_0 = -10\,k_BT$. The diffusivity is much more sensitive to disorder for attractive than for repulsive interactions. The dashed line indicates the immobilization threshold defined by $D/D_0 = 0.01$. Figure (c) shows the average number of fibers $\langle N_{\mathrm{local}} \rangle$ within a distance of $b/2$ from the particle as a function of U_0. In attractive gels the particle moves into regions of high local fiber density (and thus high $\langle N_{\mathrm{local}} \rangle$) for increasing σ_d, in repulsive gels the particle moves into regions of small $\langle N_{\mathrm{local}} \rangle$.

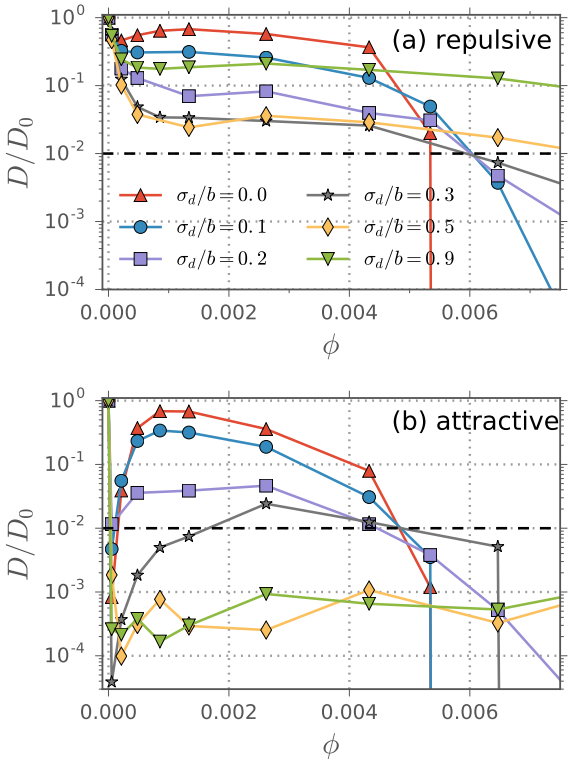

Figure 6. Particle diffusivity in interacting gels as a function of the fiber volume fraction ϕ for a fiber/particle diameter ratio $a/p = 0.05$ and large rescaled interaction range $k/s = 1.5$ for different σ_d for (a) attractive interactions with $U_0 = 10\,k_BT$ and (b) repulsive interactions with $U_0 = -10\,k_BT$. The dashed line indicates $D/D_0 = 0.01$. The interaction range is increased by a factor of 3 in comparison to fig. 5, which corresponds to a 9-fold decrease in terms of ionic strength (c.f. eq. (9)). This leads to a significant decrease in diffusivity for both attractive and repulsive U_0. Note that in (b) the data for $\sigma_d/b = 0.5$ and 0.9 exhibit large statistical errors due to limited sampling.

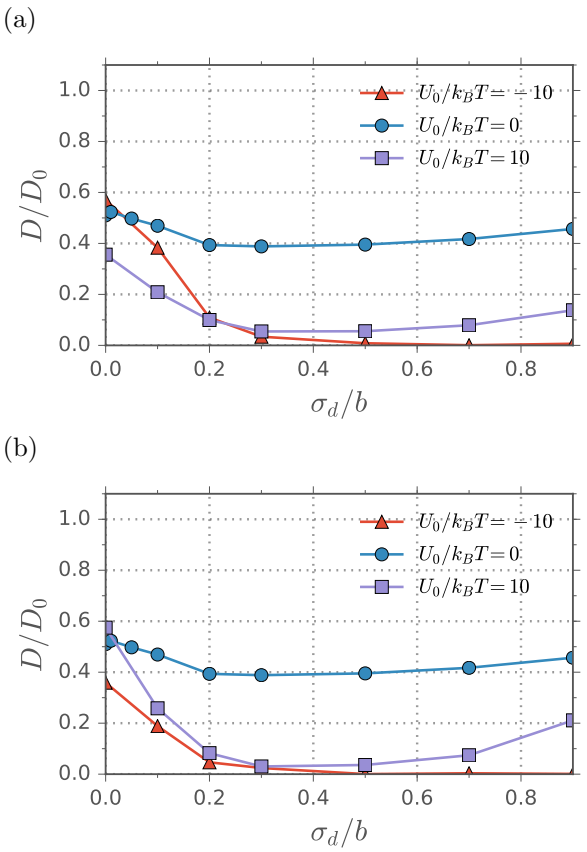

Figure 7. Particle diffusivity in interacting gels as a function of the disorder strength σ_d for $a/p = 0.05$ and a steric diameter of $s = 0.7b$ ($\phi \approx 0.003$). The rescaled interaction range is $k/s = 0.5$ for (a) and $k/s = 1.5$ for (b). The data for $U_0 \neq 0$ presented in (a) and (b) corresponds to data shown in figs. 5 and 6, respectively. Both the purely steric, $U_0 = 0$, and the repulsive case, $U_0/k_BT = 10$, exhibit a characteristic minimum around $\sigma_d/b \sim 0.3$. The attractive case, $U_0/k_BT = -10$, exhibits a monotonically decreasing diffusivity as a function of σ_d.

For attractive interactions disorder modifies trapping mechanism

For gels with attractive nonsteric interactions in figs. 5b and 6b the particle mobilities for disordered $\sigma_d/b = 0.3$ to 0.9 systems are significantly smaller than for ordered systems over almost the entire range of volume fractions ϕ. To understand this behavior, it is instructive to study the particle snap shots in fig. 8 for $\sigma_d/b = 0.9$ gels and different steric diameters $s/b = 0.5$ ($\phi = 0.0013$, bottom center) and $s/b = 0.2$ ($\phi = 0.0002$, bottom right). The particle position snap shots are from consecutive times during a single trajectory. They clearly indicate the tendency of the particle to stay in regions with locally increased fiber density during the simulation, which we refer to as *dense-region trapping*. The corresponding snap shots in ordered gels with identical k/s and U_0/k_BT are for the weakly interacting case and $\phi = 0.0013$ evenly distributed (top center) and for the strongly attractive case and $\phi = 0.0002$ (top right) clustered around the vertices where three orthogonal attractive fibers create a local potential minimum. This illustrates that the *vertex trapping* mechanism in highly ordered attractive gels is most effective for small ϕ, as also seen in figs. 5b and 6b. In order to distinguish vertex and dense-region trapping, we show in fig. 5c the average number of fibers within a distance of less than $b/2$ from the particle, $\langle N_{\text{local}} \rangle$, as a function of U_0 for $\phi = 0.0013$ ($s/b = 0.5$) and $k/s = 0.5$. For attractive interactions, $U_0 < 0$, the particle mostly stays in regions where several fibers are close together, corresponding to high $\langle N_{\text{local}} \rangle$. The completely ordered

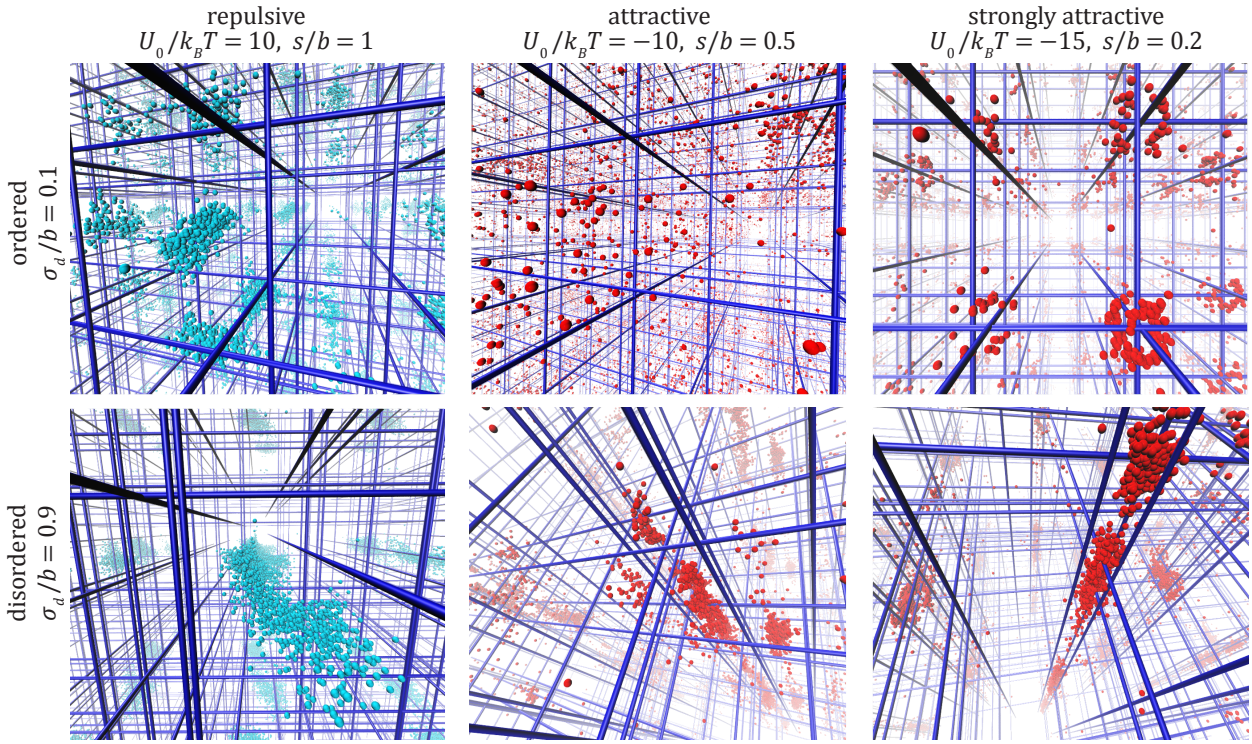

Figure 8. Particle position snap shots from a single trajectory at consecutive times (colored spheres) in ordered and disordered gels taken from simulations that have been run for the same time. The spheres indicating the particle positions are not drawn to scale. The rescaled interaction range is fixed at $k/s = 0.5$. The top row shows results for highly ordered gels with a small disorder strength $\sigma_d/b = 0.1$ while the bottom row shows results for strongly disordered gels $\sigma_d/b = 0.9$. In the left figures, the particle-fiber interaction is repulsive with $U_0\, k_BT = 10$, indicated by similarly colored spheres and fibers, and the steric diameter $s = b$ is equal to the mesh size, which corresponds to a fiber volume fraction of $\phi = 0.0053$ for $a/p = 0.05$. In the central column the fibers are attractive with $U_0/\, k_BT = -10$ and $s/b = 0.5$ ($\phi = 0.0013$). In the right figures the steric diameter is smaller, $s/b = 0.2$ ($\phi = 0.0002$), and the fibers are strongly attractive, $U_0/\, k_BT = -15$. The mean squared displacements are $\langle \Delta r^2(t)\rangle/b^2 = 3.5$ (top left), 215 (top center) and between 17 and 46 for the other figures. These figures visually demonstrate the three different trapping mechanisms, namely *exclusion trapping* (left figures) for repulsive nonsteric interactions, *vertex trapping* (top right) for ordered attractive gels and *dense-region trapping* (bottom middle and right) for disordered attractive gels.

$\sigma_d/b = 0$ gel has an upper bound of $\langle N_{\rm local}\rangle = 3$, which corresponds to three orthogonal fibers that meet at a vertex. For more disordered gels $\langle N_{\rm local}\rangle$ is significantly higher, confirming that in a disordered gel with attractive nonsteric interactions, particles are strongly immobilized in regions of high local fiber density. Lieleg and coworkers suggested that a similar effect leads to trapping of nanoparticles in the ECM, which they observed by studying single-particle trajectories of particles with a diameter comparable to the mesh size of the ECM [12]. The large difference of the trapping efficiency between vertex and dense-region trapping makes diffusion in gels with attractive nonsteric interactions particularly sensitive to spatial disorder, this is clearly demonstrated in figs. 5b and 6b.

For repulsive interaction potentials, $U_0 > 0$, in fig. 5c the particle tends to stay away from the fibers and preferentially stays in regions of small $\langle N_{\rm local}\rangle$, i.e. small local fiber density. Exclusion is reinforced in more disordered gels, since the particle can access regions with particularly small local fiber density. Figure 9 provides a schematic overview of the different trapping mechanisms for interacting gels.

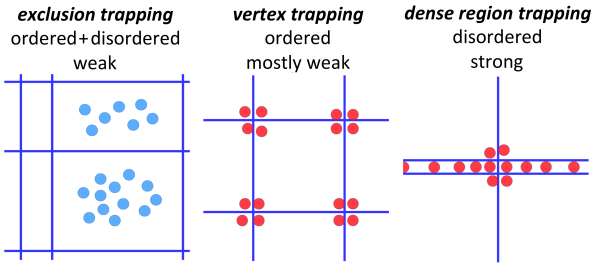

Figure 9. Schematic illustration of the different particle trapping mechanisms, namely *exclusion trapping*, *vertex trapping* and *dense-region trapping*.

4 Discussion

Particles in repulsive gels diffuse rapidly

Many experimental publications classify particles in terms of their ability to penetrate the mucus barrier, which is a desirable property for drug delivery purposes. Particles are typically classified as rapidly moving if they exhibit a relative diffusivity in mucus of more than $D/D_0 = 0.01$ [4, 10, 42, 43]. Applying this classification scheme to our results, denoted by the broken horizontal lines in figs. 5 and 6, we find that particles always diffuse rapidly in gels with repulsive nonsteric interactions in figs. 5a and 6a as long as they are smaller than the average mesh size b. This is a consequence of the comparably weak exclusion trapping mechanism. Hence, particles that interact repulsively with the gel fibers, e.g. particles that are similarly charged as the gel or particles that are charge-neutral and hydrophilic, should be suitable to for drug delivery purposes. Experimental studies for nanoparticle diffusion in mucus [5, 6, 17] and molecular dye diffusion in synthetic gels [16] arrive at the same conclusion.

Disordered gels filter interacting particles most effectively

The filtering capabilities of biopolymer gels like mucus and the ECM are of particular importance in biology. Interaction filtering can lead to the selective immobilization of a certain type of interacting particle, for example, in the ECM charged particles that interact with the fibers via electrostatic interactions are immobilized but not neutral particles [2]. For charged particles, interaction filtering can also involve filtering with respect to the sign of the charge, e.g. positively charged peptides are immobilized in porcine mucin hydrogel and negatively charged peptides are mobile [5]. Our results indicate that interaction filtering is much more effective for spatially disordered gels, than for ordered gels, since disordered gels hinder interacting particles for both interaction signs more strongly than ordered gels (c.f. fig. 7). In terms of the charge asymmetry, we find that disordered gels allow rapid diffusion for repulsive particle-gel interactions but effectively immobilize particles that are attracted to the gel by dense-region trapping. This can be seen, for example, for $\sigma_d/b \geq 0.5$ in fig. 7. For ordered gels, by contrast, exclusion trapping and vertex trapping are both comparably weak for most volume fractions, which makes them much less suitable for interaction filtering.

Ion concentration strongly impacts the diffusivity of charged particles in charged gels

According to eq. (9) the electrostatic interaction range k is related to the ion concentration as $C_{\mathrm{Ion}} \propto k^{-2}$. Hence, to appreciate how the diffusive behavior of charged particles in charged gels depends on the ion concentration, it is useful to compare our simulation data for interaction range $k/s = 0.5$ and $k/s = 1.5$, see fig. 5 and fig. 6, respectively. This increase in interaction range corresponds to a 9-fold decrease in terms of ion concentration. For repulsive interaction U_0 (figs. 5a and 6a) decreasing the ionic strength has

a significant impact. On the one hand, it significantly decreases the particle diffusivity for small volume fractions $\phi < 0.004$. On the other hand, decreasing the ionic strength qualitatively changes the diffusive behavior for all σ_d, e.g. we find a non-monotonic dependence of D on ϕ for both very ordered $\sigma_d/b = 0$ gels and disordered $\sigma_d/b = 0.9$ gels in fig. 6a, due to increasing the interaction range relative to the mesh size k/b. For ordered gels with attractive interactions in figs. 5b and 6b lowering the ionic strength causes a severe reduction in the particle mobility for small volume fractions. For disordered gels with attractive interactions, $\sigma_d/b \geq 0.5$, the diffusivity also decreases significantly for intermediate volume fractions. Thus, both vertex trapping and dense-region trapping become more pronounced for lower ionic strengths.

Comparison to experimental data for charged and neutral dextran gels

In order to quantitatively test our model predictions we compare to previously published experimental data for the diffusion of Alexa488 molecules in dextran hydrogels that were obtained by fluorescence correlation spectroscopy methods [16]. Alexa488 has a net negative charge and neutral dextran (dextran(o)), positively charged DEAE-dextran (dextran(+)) and negatively charged CM-dextran (dextran(-)) gels have been studied. Here, we compare the experimental data for the diffusivity of Alexa488 under varying dextran mass concentrations to our simulations including spatial disorder. The following model parameters are dictated by the experiment: the particle diameter is 1.48nm [16] and the polymer chain diameter is 0.74nm [44], hence we obtain a size ratio $a/p = 0.5$. Using the partial specific volume $\nu_s = 0.61$mL/g [44] for dextran, we calculate the fiber volume fraction from the polymer concentration C_{poly} in wt% as $\phi = C_{\text{poly}} \times 0.0061$. To calculate the electrostatic interaction range k using eq. (9), one has to note that the experiments were performed in buffer solution with an ion concentration of 10 mM. Furthermore, one has to take into account the ionic strength of the counterions that enter the solution upon addition of dextran(-) and dextran(+), which effectively renders the interaction range k dependent on ϕ. Increasing ϕ by 0.01 corresponds to an increase in ion concentration by 3.66mM and 6.1mM for dextran(-) and dextran(+), respectively [16]. We use the interaction potential strength U_0 as a fit parameter, but constrain the ratio of the potential strength for dextran(+) and dextran(-) to be equal to the dextran charge ratio, which is 5/3 [16]. Figure 10a shows a comparison of experimental data (unconnected symbols) and simulation data (filled, connected symbols) for disordered $\sigma_d/b = 0.9$ gels with a neutral, an attractive and a repulsive interaction potential, $U_0 = 0$, $U_0/\,k_BT = -8$ and $U_0/\,k_BT = 4.8$, respectively. The simulation and experimental data show similar trends. For the attractive case, that means negative Alexa488 in positive dextran(+), the diffusivities increase with the fiber volume fraction ϕ. This at first sight surprising result can be rationalized by the fact that the salt concentration increases with rising ϕ and thus the electrostatic interaction range goes down as ϕ goes up. For the repulsive case of Alexa488 in negative dextran(-) the diffusivities decrease with ϕ, but the simulation diffusivities are significantly lower than the experimental data. The simulation data for the neutral case show a significantly higher diffusivity than for the repulsive case. This stands in contrast to the experimental data for Alexa488 in neutral dextran20(o) (20 kDa molecular weight) and neutral dextran500(o) (500 kDa), that show similar D/D_0 as for the repulsive dextran(-) case, indicating that in the experiment the effect of repulsive charges is significantly weaker than in our simulation model. This could be due to fiber flexibility, which is neglected in our simulation model, as will be discussed further below.

In the comparison between experimental and simulation data for an ordered $\sigma_d = 0$ gel in fig. 10b, the simulation data significantly deviates from the experimental data for the attractive case. We conclude that our disordered gel model describes the experimental situation better than an ordered cubic lattice model, in accordance to neutral dextran gels, which form disordered polymer systems [41, 45]. Note that we use the fitted interaction potential strengths of $U_0/k_BT = -12$ and $U_0/k_BT = 7.2$ in fig. 10b. A plot

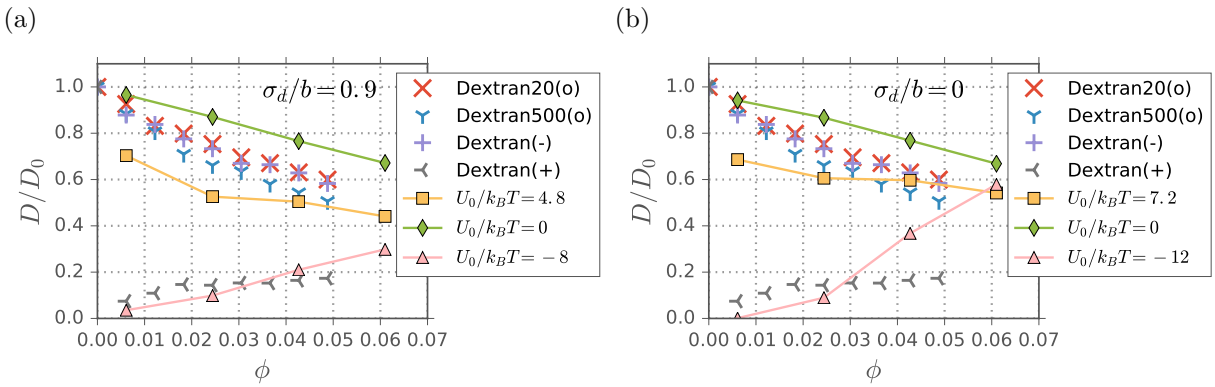

Figure 10. Comparison of particle diffusivity as a function of the fiber volume fraction ϕ from simulations for interacting gels (filled connected symbols) with experimental data for Alexa488 diffusion in different dextran hydrogels (unconnected symbols). The simulations use a fiber/particle diameter ratio $a/p = 0.5$ and a disorder strength of (a) $\sigma_d/b = 0.9$ and (b) $\sigma_d = 0$. The interaction range k is dictated by the experimental ionic strength as described in the text. The experimental data was obtained by fluorescence correlation spectroscopy in 10 mM buffer solution with a free solution diffusivity of $D_0 = 320\mu m/s^2$ [16]. We find qualitative agreement between simulations and experimental data for $\sigma_d/b = 0.9$ in (a). For $\sigma_d = 0$ in (b), the data for attractive fibers disagree.

using $U_0/\ k_BT = -8$ and $U_0/\ k_BT = 4.8$ like in fig. 10a for the ordered gel with $\sigma_d = 0$ is shown in the supplementary information in fig. S3. In our previous paper [16], we obtained qualitative agreement between simulations for an ordered gel model with $\sigma_d = 0$ and experimental data for Alexa488 diffusion in dextran(+) and dextran(-) as a function of added salt at a low fiber volume fraction of $\phi = 0.006$ (C_{poly} =1wt%). In that comparison the agreement between simulation and experiment was particularly good for intermediate to large salt concentrations, but for small salt concentrations, our ordered model underestimated the diffusivity. This is in agreement with our results in fig. 10b, where it is seen that the ordered model significantly underestimates the diffusivity for $\phi = 0.006$.

There are a number of potential reasons for the deviations between the experimental data and our model results in fig. 10a. First, our model might overestimate the strength of repulsive electrostatic interactions, since we approximate the discrete charges along the dextran polymers by a constant line charge density. The 1.48nm-sized Alexa488 molecules might be able to avoid the discrete repulsive charges on a dextran(-) polymer rather effectively, as their spacing is on average five times the dextran monomer width $5 \times 0.4\text{nm} = 2\text{nm}$ [44]; in this estimate we used the fact that only about one in five dextran monomers carries a charged carboxyl group [16]. Secondly, dextran polymers are flexible [41] and, thus, are in principle able to move away from a similarly charged particle and towards an oppositely charged particle, which would effectively weaken the electrostatic repulsion in the experiment and, conversely, increase the electrostatic attraction. Thirdly, the increasing concentrations of dextran(+) and dextran(-) might change the pH of the gel solution enough to influence the number of charged amino and carboxyl groups on the dextran(+) and dextran(-) polymers, according to their respective pK_a and pK_b values. Finally, the Alexa488 molecule has an inhomogeneous charge distribution with three negative charges and one positive charge, which might affect its diffusivity in charged gels [5]. Hence, it is likely that the electrostatic interaction between the polymer chains and an Alexa488 particle is more complex than we capture with our simplified interaction potential eq. (8). Nevertheless, we find that our approximative, coarse-grained interacting gel model qualitatively reproduces the basic experimental trends.

5 Conclusions

We present a model to investigate the trapping mechanisms of nanoparticles in spatially disordered gels with attractive or repulsive nonsteric particle-gel interactions. By changing the disorder strength σ_d we generate ordered as well disordered gels. We find that particles are generally more strongly trapped in spatially disordered than in ordered gels. We observe three distinct trapping mechanisms. In gels with repulsive nonsteric interactions particle diffusion is hindered through exclusion trapping. The particle is confined to regions with small local fiber density and an optimal trapping capacity is achieved for an intermediate degree of disorder (c.f. figs. 5a and 6a), since the particle can cross between cells in an almost unhindered fashion for low σ_d as well as for high σ_d. Diffusion in gels with repulsive nonsteric interactions is similar to diffusion in purely steric gels, which also achieve an optimal trapping capacity for an intermediate degree of disorder (c.f. fig. 3). For gels with attractive nonsteric interactions, disorder influences particle diffusion much more severely than for gels with repulsive interactions, and we find two distinct trapping mechanisms for ordered and disordered gels (c.f. fig. 9). In ordered gels, vertex trapping occurs, which is most effective for small fiber volume fractions. Thus, diffusion in ordered gels with attractive nonsteric interactions exhibits a peculiar non-monotonic dependence on ϕ (c.f. figs. 5b and 6b). Even a small degree of spatial disorder eliminates these non-monotonic effects, so to see them in experiments one would need spatially ordered gel structures as can be produced by DNA origami techniques [46]. In disordered gels with attractive nonsteric interactions we find dense-region trapping, which is the most effective immobilization mechanism. Here the particle is trapped in regions of high local fiber density, i.e. near several proximate fibers which create a deep valley in the potential landscape. A similar mechanism has previously been suggested on the basis of experimental data for the ECM [12] and mucus [3]. Numerous experimental results show that gels with attractive nonsteric particle-gel interactions filter nanoparticles much more effectively than gels with repulsive nonsteric particle-gel interactions [5–7, 16, 17]. We argue that this is due to the dense-region trapping mechanism, since we expect considerable spatial disorder in polymer gels [19, 21, 29, 30, 41, 47, 48].

Reducing the ion concentration by about an order of magnitude, i.e. increasing the electrostatic interaction range k by a factor of three between fig. 5 and fig. 6, severely enhances the effect of dense-region trapping in disordered gels with attractive electrostatic interactions, which makes the ionic strength a useful parameter to regulate charged particle mobility in charged gels [2, 5, 11, 16]. More systematic experimental research on the effects of ionic strength on diffusion in electrostatically interacting gels would be desirable.

We neglect the effect of flexibility of the polymer lattice in our simulations. Theoretical research has shown that for purely steric systems, network flexibility increases the particle diffusivity compared to static networks, in particular for large particles [49, 50]. In our simulations, the fibers are rigid, but the network is not static for disordered lattices. However, flexibility may mitigate the differences between ordered and disordered lattices. For future work, it would be interesting to examine the effect of flexibility for gels with nonsteric particle-gel interactions. Furthermore, we neglect that the polymer chains inside a gel have a finite length and we assume that it would not qualitatively change our results: For purely steric gels, we assume that the fiber length, just like the degree of spatial disorder (c.f. fig. 3b), will not have a large effect on the diffusive behavior of particles smaller than the mesh size. In the presence of repulsive nonsteric interactions exclusion trapping will likely hardly be affected by the fiber length, since the particle avoids the fibers. For attractive nonsteric interactions, we assume that dense-region trapping will have qualitatively the same effect on the diffusivity as for infinitely long fibers.

A great deal of pharmaceutical research is directed towards elucidating the barrier properties of biogels like mucus and the ECM. Our simulations indicate how polymer gels filter interacting particles regarding the sign and strength of their interaction. Attractive, e.g. oppositely charged, particles are immobilized

and repulsive particles can rapidly traverse biopolymer layers like the mucus barriers, regardless of the fiber lattice geometry, as long as they are smaller than the average mesh size. The highest mobilities for particles in gels are of course achieved for inert particles, i.e. when no nonsteric particle-fiber interactions slow down the particle [2, 8–10, 20, 42, 43]. These insights can be used for the design of advanced drug delivery techniques with nanoparticle carriers through biogel layers. For example, large particles are considered particularly useful for drug delivery purposes since they are more suitable for drug loading and release than smaller particles [4]. In agreement to [20], our simulations show that large particles with a diameter comparable to the mesh size, which can be on the order of 1µm in biogels [4,12], are mobile in repulsive disordered gels, even for small ion concentrations in the presence of strong repulsive nonsteric particle-gel interactions, (c.f. fig. 6a) since the particle readily avoids the repulsive fibers. On the other hand, large particles in attractive gels are immobilized due to dense-region trapping. Thus, in order to achieve rapid diffusion of large nanoparticles through a biopolymer barrier they should be electrostatically repulsive towards the fibers, i.e. oppositely charged, or they should be charge neutral and hydrophilic.

Acknowledgements

The manuscript was written through contributions of all authors.J.H. performed research. J.H. and R.R.N. designed research, analyzed data, and wrote the article. This work was supported by the Deutsche Forschungsgemeinschaft via grant GRK1558.

References

[1] O. Lieleg and K. Ribbeck, "Biological hydrogels as selective diffusion barriers.," *Trends in cell biology*, vol. 21, pp. 543–51, sep 2011.

[2] O. Lieleg, R. Baumgärtel, and A. Bausch, "Selective filtering of particles by the extracellular matrix: an electrostatic bandpass," *Biophysical journal*, vol. 97, pp. 1569–77, sep 2009.

[3] Q. Xu, N. J. Boylan, J. S. Suk, Y.-Y. Wang, E. A. Nance, J.-C. Yang, P. J. McDonnell, R. A. Cone, E. J. Duh, and J. Hanes, "Nanoparticle diffusion in, and microrheology of, the bovine vitreous ex vivo," *Journal of Controlled Release*, vol. 167, no. 1, pp. 76–84, 2013.

[4] S. K. Lai, D. E. O'Hanlon, S. Harrold, S. T. Man, Y.-Y. Wang, R. Cone, and J. Hanes, "Rapid transport of large polymeric nanoparticles in fresh undiluted human mucus," *Proceedings of the National Academy of Sciences of the United States of America*, vol. 104, no. 5, pp. 1482–1487, 2007.

[5] L. D. Li, T. Crouzier, A. Sarkar, L. Dunphy, J. Han, and K. Ribbeck, "Spatial Configuration and Composition of Charge Modulates Transport into a Mucin Hydrogel Barrier," *Biophysical Journal*, vol. 105, no. 6, pp. 1357–1365, 2013.

[6] B. T. Käsdorf, F. Arends, and O. Lieleg, "Diffusion Regulation in the Vitreous Humor.," *Biophysical journal*, vol. 109, pp. 2171–81, nov 2015.

[7] L. Rusu, D. Lumma, and J. O. Rädler, "Charge and size dependence of liposome diffusion in semidilute biopolymer solutions.," *Macromolecular bioscience*, vol. 10, pp. 1465–72, dec 2010.

[8] F. Laffleur, F. Hintzen, G. Shahnaz, D. Rahmat, K. Leithner, and A. Bernkop-Schnürch, "Development and in vitro evaluation of slippery nanoparticles for enhanced diffusion through native mucus," *Nanomedicine*, vol. 9, pp. 387–396, mar 2014.

[9] M. Abdulkarim, N. Agulló, B. Cattoz, P. Griffiths, A. Bernkop-Schnürch, S. G. Borros, and M. Gumbleton, "Nanoparticle diffusion within intestinal mucus: Three-dimensional response analysis dissecting the impact of particle surface charge, size and heterogeneity across polyelectrolyte, pegylated and viral particles," *European Journal of Pharmaceutics and Biopharmaceutics*, vol. 97, pp. 230–238, nov 2015.

[10] Y. Wang, S. Lai, and J. Suk, "Addressing the PEG mucoadhesivity paradox to engineer nanoparticles that "slip" through the human mucus barrier," *Angewandte Chemie International Edition*, pp. 9726–9729, 2008.

[11] O. Lieleg, I. Vladescu, and K. Ribbeck, "Characterization of particle translocation through mucin hydrogels," *Biophysical journal*, vol. 98, pp. 1782–9, may 2010.

[12] F. Arends, R. Baumgärtel, and O. Lieleg, "Ion-specific effects modulate the diffusive mobility of colloids in an extracellular matrix gel.," *Langmuir : the ACS journal of surfaces and colloids*, vol. 29, pp. 15965–73, dec 2013.

[13] R. G. Thorne, A. Lakkaraju, E. Rodriguez-Boulan, and C. Nicholson, "In vivo diffusion of lactoferrin in brain extracellular space is regulated by interactions with heparan sulfate.," *Proceedings of the National Academy of Sciences of the United States of America*, vol. 105, pp. 8416–21, jun 2008.

[14] A. Birjiniuk, N. Billings, E. Nance, J. Hanes, K. Ribbeck, and P. S. Doyle, "Single particle tracking reveals spatial and dynamic organization of the Escherichia coli biofilm matrix," *New Journal of Physics*, vol. 16, no. 8, p. 085014, 2014.

[15] L. J. Colwell, M. P. Brenner, and K. Ribbeck, "Charge as a selection criterion for translocation through the nuclear pore complex.," *PLoS computational biology*, vol. 6, p. e1000747, apr 2010.

[16] X. Zhang, J. Hansing, R. R. Netz, and J. E. DeRouchey, "Particle Transport through Hydrogels Is Charge Asymmetric.," *Biophysical journal*, vol. 108, pp. 530–9, feb 2015.

[17] J. S. Crater and R. L. Carrier, "Barrier Properties of Gastrointestinal Mucus to Nanoparticle Transport," *Macromolecular Bioscience*, vol. 10, pp. 1473–1483, dec 2010.

[18] J. Hansing, C. Ciemer, W. K. Kim, X. Zhang, J. E. DeRouchey, and R. R. Netz, "Nanoparticle filtering in charged hydrogels: Effects of particle size, charge asymmetry and salt concentration," *The European Physical Journal E*, vol. 39, no. 5, p. 53, 2016.

[19] T. Stylianopoulos, B. Diop-Frimpong, L. L. Munn, and R. K. Jain, "Diffusion anisotropy in collagen gels and tumors: the effect of fiber network orientation.," *Biophysical journal*, vol. 99, pp. 3119–28, nov 2010.

[20] T. Stylianopoulos, M.-Z. Poh, N. Insin, M. G. Bawendi, D. Fukumura, L. L. Munn, and R. K. Jain, "Diffusion of particles in the extracellular matrix: the effect of repulsive electrostatic interactions.," *Biophysical journal*, vol. 99, pp. 1342–9, sep 2010.

[21] J. Kirch, A. Schneider, B. Abou, A. Hopf, U. F. Schaefer, M. Schneider, C. Schall, C. Wagner, and C.-M. Lehr, "Optical tweezers reveal relationship between microstructure and nanoparticle penetration of pulmonary mucus.," *Proceedings of the National Academy of Sciences of the United States of America*, vol. 109, pp. 18355–60, nov 2012.

[22] A. Godec, M. Bauer, and R. Metzler, "Collective dynamics effect transient subdiffusion of inert tracers in flexible gel networks," *New Journal of Physics*, vol. 16, p. 092002, sep 2014.

[23] S. K. Ghosh, A. G. Cherstvy, and R. Metzler, "Non-universal tracer diffusion in crowded media of non-inert obstacles.," *Physical chemistry chemical physics : PCCP*, vol. 17, pp. 1847–58, jan 2015.

[24] T. Miyata, "Brownian Dynamics Simulation of Self-Diffusion of Ionic Large Solute Molecule in Modeled Polyelectrolyte Gel," *Journal of the Physical Society of Japan*, vol. 81, p. SA010, nov 2012.

[25] H. Zhou and S. Chen, "Brownian dynamics simulation of tracer diffusion in a cross-linked network," *Physical Review E*, vol. 79, p. 021801, feb 2009.

[26] A. Wedemeier, H. Merlitz, C.-X. Wu, and J. Langowski, "Modeling diffusional transport in the interphase cell nucleus," *The Journal of Chemical Physics*, vol. 127, no. 4, p. 045102, 2007.

[27] H. Masoud and A. Alexeev, "Permeability and Diffusion through Mechanically Deformed Random Polymer Networks," *Macromolecules*, vol. 43, pp. 10117–10122, dec 2010.

[28] J. Israelachvili, *Intermolecular and Surface Forces*. Intermolecular and Surface Forces, Elsevier Science, 2010.

[29] S. Lai, Y. Wang, D. Wirtz, and J. Hanes, "Micro-and macrorheology of mucus," *Advanced drug delivery reviews*, vol. 61, no. 2, pp. 86–100, 2009.

[30] E. M. Johnson, D. A. Berk, R. K. Jain, and W. M. Deen, "Hindered diffusion in agarose gels: test of effective medium model.," *Biophysical journal*, vol. 70, pp. 1017–23, feb 1996.

[31] R. J. Phillips, "A hydrodynamic model for hindered diffusion of proteins and micelles in hydrogels.," *Biophysical journal*, vol. 79, pp. 3350–3, dec 2000.

[32] S. Seiffert and W. Oppermann, "Diffusion of linear macromolecules and spherical particles in semidilute polymer solutions and polymer networks," *Polymer*, vol. 49, no. 19, pp. 4115–4126, 2008.

[33] G. D. J. Phillies, "The hydrodynamic scaling model for polymer self-diffusion," *The Journal of Physical Chemistry*, vol. 93, pp. 5029–5039, jun 1989.

[34] A. Michelman-Ribeiro, F. Horkay, R. Nossal, and H. Boukari, "Probe diffusion in aqueous poly(vinyl alcohol) solutions studied by fluorescence correlation spectroscopy.," *Biomacromolecules*, vol. 8, pp. 1595–600, may 2007.

[35] G. Modesti, B. Zimmermann, M. Börsch, A. Herrmann, and K. Saalwächter, "Diffusion in Model Networks as Studied by NMR and Fluorescence Correlation Spectroscopy.," *Macromolecules*, vol. 42, pp. 4681–4689, jul 2009.

[36] R. J. Phillips, W. M. Deen, and J. F. Brady, "Hindered transport of spherical macromolecules in fibrous membranes and gels," *AIChE Journal*, vol. 35, pp. 1761–1769, nov 1989.

[37] R. J. Phillips, W. M. Deen, and J. F. Brady, "Hindered transport in fibrous membranes and gels: Effect of solute size and fiber configuration," *Journal of Colloid and Interface Science*, vol. 139, pp. 363–373, oct 1990.

[38] D. S. Clague and R. J. Phillips, "Hindered diffusion of spherical macromolecules through dilute fibrous media," *Physics of Fluids*, vol. 8, p. 1720, jul 1996.

[39] J. Tong and J. L. Anderson, "Partitioning and diffusion of proteins and linear polymers in polyacrylamide gels.," *Biophysical journal*, vol. 70, pp. 1505–13, mar 1996.

[40] I. H. Park, C. S. Johnson, and D. A. Gabriel, "Probe diffusion in polyacrylamide gels as observed by means of holographic relaxation methods: search for a universal equation," *Macromolecules*, vol. 23, pp. 1548–1553, sep 1990.

[41] B. Amsden, "Solute Diffusion within Hydrogels. Mechanisms and Models," *Macromolecules*, vol. 31, pp. 8382–8395, nov 1998.

[42] B. S. Schuster, J. S. Suk, G. F. Woodworth, and J. Hanes, "Nanoparticle diffusion in respiratory mucus from humans without lung disease," *Biomaterials*, vol. 34, no. 13, pp. 3439–3446, 2013.

[43] S. K. Lai, J. S. Suk, A. Pace, Y.-Y. Wang, M. Yang, O. Mert, J. Chen, J. Kim, and J. Hanes, "Drug carrier nanoparticles that penetrate human chronic rhinosinusitis mucus.," *Biomaterials*, vol. 32, pp. 6285–90, sep 2011.

[44] L. Johansson, C. Elvingson, and J. E. Loefroth, "Diffusion and interaction in gels and solutions. 3. Theoretical results on the obstruction effect," *Macromolecules*, vol. 24, pp. 6024–6029, oct 1991.

[45] W. Hennink, H. Talsma, J. Borchert, S. De Smedt, and J. Demeester, "Controlled release of proteins from dextran hydrogels," *Journal of Controlled Release*, vol. 39, no. 1, pp. 47–55, 1996.

[46] C. E. Castro, F. Kilchherr, D.-N. Kim, E. L. Shiao, T. Wauer, P. Wortmann, M. Bathe, and H. Dietz, "A primer to scaffolded DNA origami," *Nature Methods*, vol. 8, pp. 221–229, mar 2011.

[47] X. Yang, K. Forier, L. Steukers, S. Van Vlierberghe, P. Dubruel, K. Braeckmans, S. Glorieux, and H. J. Nauwynck, "Immobilization of pseudorabies virus in porcine tracheal respiratory mucus revealed by single particle tracking.," *PloS one*, vol. 7, p. e51054, jan 2012.

[48] Y. Cu and W. M. Saltzman, "Mathematical modeling of molecular diffusion through mucus," *Advanced Drug Delivery Reviews*, vol. 61, no. 2, pp. 101–114, 2009.

[49] A. Wedemeier, H. Merlitz, C.-X. Wu, and J. Langowski, "How proteins squeeze through polymer networks: A Cartesian lattice study," *The Journal of Chemical Physics*, vol. 131, no. 6, p. 064905, 2009.

[50] N. Kamerlin and C. Elvingson, "Tracer diffusion in a polymer gel: simulations of static and dynamic 3D networks using spherical boundary conditions," *Journal of Physics: Condensed Matter*, vol. 28, p. 475101, nov 2016.